Partial retention of ancient function increases genetic pleiotropy in grass evolution

Authors: Amber de Neve, Olivia Kelly, Terice Kelly, Sam Leiboff, Madelaine Bartlett

Abstract:

Changes in form are driven by the differential, context-dependent regulation of pleiotropic genes. How genetic pleiotropy itself emerges, however, remains unclear. The maize genes *GRASSY TILLERS1* (*GT1*) and *RAMOSA3* (*RA3*) are required for axillary meristem suppression, a deeply conserved trait across angiosperms, and for floral organ suppression, a trait which evolved within the grass family. To determine how these pleiotropic functions are regulated, we first established a high-throughput method for quantitative phenotyping of grass flowers. Using this method, we show that distinct environmental mechanisms regulate axillary meristem versus floral organ suppression. In line with these differences, we find upstream regulation of *GT1* and *RA3* has diverged, consistent with their redeployment in flowers. Our results show that, rather than wholesale adoption of genetic networks, developmental genes can retain ancient functions *and* be recruited into other programs in the evolution of form, thereby increasing genetic pleiotropy.

Intro:

Rather than generating new proteins through coding sequence changes, morphological evolution often arises from changes in when and where proteins are expressed (King and Wilson 1975; Carroll 2005). Mutations that impact gene expression instead of protein structure can generate evolutionary novelty while minimizing harmful side effects, thus reducing the risk of negative mutational pleiotropy from drastic changes to protein coding sequences (Prud'homme, Gompel, and Carroll 2007). Pleiotropy - the influence of a single locus on multiple traits - exists in two forms: mutational pleiotropy, where single base pair substitutions, insertions, or deletions affect multiple genetic functions; and genetic pleiotropy, in which null mutations abolish all functions of a gene (Stearns 2010); (Zhang 2023). While both mutational and genetic pleiotropy can be positive (or adaptive) for evolution (Foster et al. 2004; Hämälä et al. 2020; Kostyun et al. 2019), negative (or antagonistic) pleiotropy occurs when evolution is constrained due to phenotypic effects that both increase and decrease fitness (Zhang 2023). As the number and complexity of traits influenced by pleiotropy increase, beneficial mutations become less likely, as positive effects get diluted by unwanted negative side effects on other traits (H. A. Orr 2000; Welch and Waxman 2003). This layered complexity often obscures the origins of pleiotropy, which remain difficult to pinpoint.

Pleiotropy may emerge from the same genetic modules being redeployed to shape morphology. For example, parts of the genetic program regulating lateral branch initiation in maize are recruited to promote the growth of the leaf ligule, a specialized hinge structure at the sheath-blade boundary (Johnston et al. 2014; Bertolini et al. 2025). While in this case module redeployment promotes growth, in other contexts modules can be co-opted to suppress it.

In maize, two pleiotropic genes involved in growth suppression are *GRASSY TILLERS1* (*GT1*) and *RAMOSA3* (*RA3*) (Whipple et al. 2011; Satoh-Nagasawa et al. 2006; Klein et al. 2022). *GT1* controls selective pistil suppression in maize tassel flowers, a process that is essential to form unisexual staminate flowers (Whipple et al. 2011). Unisexual flowers in the maize tassel start development as bisexual, then pistil primordia undergo cell death leaving behind only the stamens (Calderon-Urrea and Dellaporta 1999). Besides its role in flower development, *GT1* is also an important regulator of tillering (or axillary branching) (Whipple et al. 2011). *gt1* mutants have pistils in tassel florets, as well as additional tiller branches and husk leaves (Whipple et al. 2011). *RA3* also affects both branching and floral development and encodes a trehalose-6-phosphate (Tre6P) phosphatase (Satoh-Nagasawa et al. 2006; Klein et al. 2022). Notably, *ra3* mutants in a *gt1* background have increased tiller branching compared to *gt1* alone, and fully derepressed pistils in both the tassel and the ear (Klein et al. 2022). Both GT1 and Tre6P phosphatases like RA3 have ancient roles in regulating tiller suppression. *GT1* homologs suppress tiller branching in brachypodium, rice, and arabidopsis (Gallagher et al. 2023; Kumar et al. 2021; Sánchez-Gerschon et al. 2024). Similarly, Tre6P phosphatases like RA3 regulate branching across species - increased Tre6P phosphatase expression decreases branching in the arabidopsis vasculature (Fichtner et al. 2021), and Tre6P influences branch bud outgrowth initiation in garden pea (Fichtner et al. 2017). Together, *GT1* and *RA3* demonstrate how conserved modules can shape plant form, through their effects on both floral development and tillering.

The evolutionary history of pistil suppression versus tiller suppression is known. Growth suppression of lateral vegetative buds (including grass tillers) is a conserved trait in the angiosperms (Aguilar-Martínez, Poza-Carrión, and Cubas 2007; Martín-Trillo et al. 2011; Dixon et al. 2018; Takeda et al. 2003), while growth suppression of floral organs is derived. Programmed cell death of pistils likely emerged in a lineage leading to the Andropogoneae, the tribe to which maize belongs (Le Roux and Kellogg 1999). Because these two suppression phenotypes occur within the same organism, regulated by the same genes, this is an ideal system to examine how many components of the genetic module governing tiller suppression in maize are conserved within pistil suppression.

In tillering, environmental signals, particularly light and sugar availability, play critical roles in regulating branch suppression (F. F. Barbier, Lunn, and Beveridge 2015; F. Barbier et al. 2015; Patil et al. 2022; Demotes-Mainard et al. 2016), but environmental effects on pistil growth are less clear. *TEOSINTE BRANCHED1 (TB1)* integrates these environmental signals to suppress tillering (Doebley, Stec, and Gustus 1995; Kebrom, Burson, and Finlayson 2006). *TB1* is induced by shade in sorghum and arabidopsis (Kebrom, Burson, and Finlayson 2006; González-Grandío et al. 2013), and *TB1* in pea plants is downregulated when bud growth is activated by sucrose (Mason et al. 2014). Notably, *GT1* is a downstream target of TB1 in maize, and TB1 binding peaks are located near *RA3*, which is also downregulated in *tb1* mutants (Dong et al. 2019). *GT1* expression in tillers is induced by shade through TB1 (Whipple et al. 2011; González-Grandío et al. 2017). The TB1-*GT1* interaction is deeply conserved (González-Grandío et al. 2017), as is environmental plasticity of branching (Rameau et al. 2014; Z. Luo, Janssen, and Snowden 2021). Environmental conditions can also affect pistil

suppression (Qian et al. 2025; Nuccio et al. 2015), but whether the same stressors and upstream regulators as in tillering are involved is uncertain.

To assess whether TB1 and environmental signals are upstream of pistil suppression as they are in tillers, we developed a sensitive, high-throughput method that can identify subtle morphological changes in pistils. By examining the impact of defoliation and *tb1* mutant combinations on pistil development, we uncover how novel pleiotropies might emerge.

Results:

X-ray imaging paired with automated segmentation captures pistil shape data at scale

Measuring maize pistils has been difficult, because each pistil needed to be dissected out of the spikelet. To address this problem and to investigate the effects of the environment on sporophytic sex determination in maize, we developed a method that combines x-ray imaging and machine learning-based segmentation to measure pistils. First, we grew maize plants and collected the lowest tassel branch when the anthers emerged from the spikelets (Fig. 1A). We chose this collection point 1) to standardize inflorescence maturity, and 2) when the anthers are outside of the spikelet, pistils are clearer on the x-ray image. Next, we loaded the tassel branch into the x-ray CT (Computed Tomography) machine. Because the pistil tissue has high density compared to the surrounding spikelet and branch tissue, the pistils absorb more x-rays and are distinguishable as dark circles on the image (Fig. 1B). Instead of reconstructing full 3D volumes, we collected 2D x-ray scans from a reduced number of angles. This approach not only reduced scan time (<5 minutes per tassel branch), but also produced higher-quality images for CNN segmentation than 3D reconstructions, enabling more accurate detection of pistils.

Next, we trained a Mask-RCNN (Region-based Convolutional Neural Network) model to automatically measure pistils from the x-ray images (He et al. 2017). Mask-RCNN can detect objects in an image and generate segmentation masks of those objects (Fig. 1C). To train the model, we first generated a training data set of 664 x-ray images, including maize mutants with defects in tassel pistil repression and samples of *Setaria viridis*, a grass where pistils are not repressed under normal conditions (Supplemental Table 1). By incorporating *Setaria*, we built an evolutionarily informed model with enhanced applicability across grasses. We validated the performance of the model (Supplemental Fig. 1, Supplemental Table 2-3), and determined that applying a confidence threshold of 0.82 maximized the precision (fraction of correct predictions out of all predictions) and recall (fraction of correctly identified positives out of all positives) (Rainio, Teuho, and Klén 2024) of high overlap predictions (Supplemental Fig. 1). At the 0.82 confidence threshold, the median Intersection over Union (IoU), a measure of overlap between predicted and ground truth segmentations, was 0.83 (IQR = 0.73 - 0.89), indicating high accuracy for the majority of the predicted pistil segmentations (Supplemental Fig. 1). The model achieved an average precision (AP) of 0.96 at an IoU threshold of 0.50 (AP_{50}), and a mean average precision (mAP) of 0.70 across IoU thresholds from 0.50 to 0.95 in 0.05 increments (Supplemental Fig. 1). Importantly, the model generalized across multiple genotypes,

developmental stages, and species, suggesting that we produced a robust tool for quantifying pistil growth in grasses.

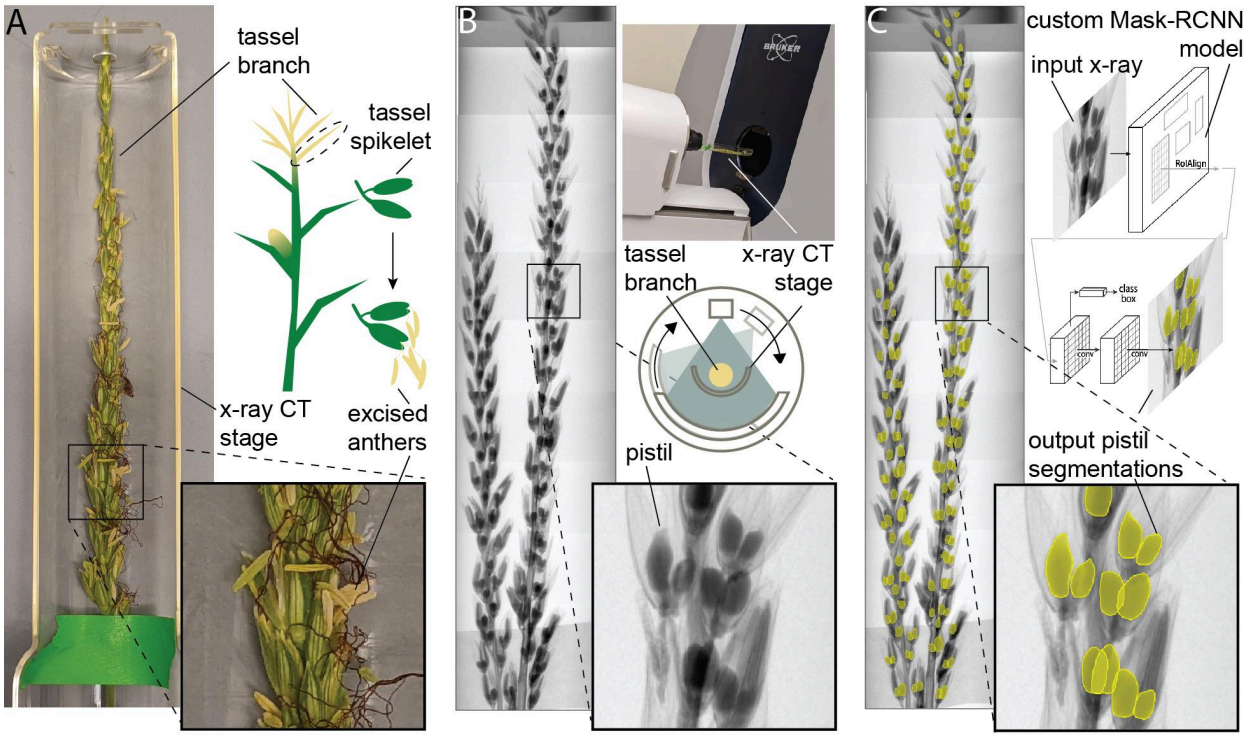

Figure 1. X-ray imaging and automated segmentation makes internal floral morphology easier to see and measure. A) The bottom tassel branch of a maize plant is collected when anthers are fully emerged from spikelets, and taped to the x-ray CT stage. This example is of a *gt1 ra3* maize plant. B) The branch is loaded horizontally into the x-ray CT machine and scans are collected along the length of the sample. Whole tassel image shows stitched individual scans. C) Scans are run through a custom trained Mask-RCNN model to segment pistils. Data from masks are used in subsequent statistical analysis. Model figure is modified from (He et al. 2017).

Mutant pistils are morphologically varied, and pistil size is affected by position on the tassel branch

We first used our new method to see what types of morphological patterns we could find in the data. We grew *gt1-P* and *gt1;ra3* mutants in the field and x-rayed tassel branches for analysis. To analyze pistil differences by position, we looked at the distal-proximal position of the pistil on the tassel branch. All tassel branch lengths were normalized to 1, and pistil position ranged between 0 at the base - 1 at the tip (Fig. 2A). We looked at pistil presence/absence across the branch in both *gt1-P* and *gt1;ra3* mutants. We found that ectopic derepressed pistils were present across the whole length of the branch for both genotypes, with fewer pistils found at the top 10% of the branches (Fig. 2B). *gt1-P* mutants often had just one visible derepressed pistil per spikelet compared to *gt1;ra3* mutants which most often had two clearly visible pistils per

spikelet (Fig. 2A, B). Along with fewer pistils, *gt1-P* tassel branches had fewer total spikelets per branch than *gt1;ra3* (Fig. 2B), likely due to a difference in branch length.

Next, using just the *gt1;ra3* dataset, we looked at pistil size along the branch. We found that pistils at the base of the branch are larger than those at the top (base pistils = 0.106 cm^2 ± 0.002; top pistils = 0.084 cm^2 ± 0.004) (Fig. 2C). This is reminiscent of several Ranunculus and orchid species, where distal flowers are smaller than proximal flowers on branches, and some distal flowers are unable to set fruit (Diggle 1995). Along with positional variability across the tassel branch, we also found there is variation in pistil size within the spikelet (Fig. 2D,E). Tassel spikelets have two unisexual staminate flowers with suppressed pistils, whereas in *gt1;ra3* plants both pistils develop (Klein et al. 2022). To measure differences at the spikelet level, we isolated all pistil pairs (see Methods). One pistil of the pair was on average ~25% smaller than the other (pistil 1 = 0.114 cm^2 ± 0.002; pistil 2 = 0.083 cm^2 ± 0.002) (Fig. 2D,E). This is consistent with previous data showing maize upper floret anthers are roughly twice the size of the lower floret anthers within a spikelet at any point on the tassel (Egger and Walbot 2015). The upper floret is larger and develops about a day ahead of the lower floret, and genes are differentially expressed between the two floret types (Yang et al. 2022), suggesting upper and lower florets may have developmental differences.

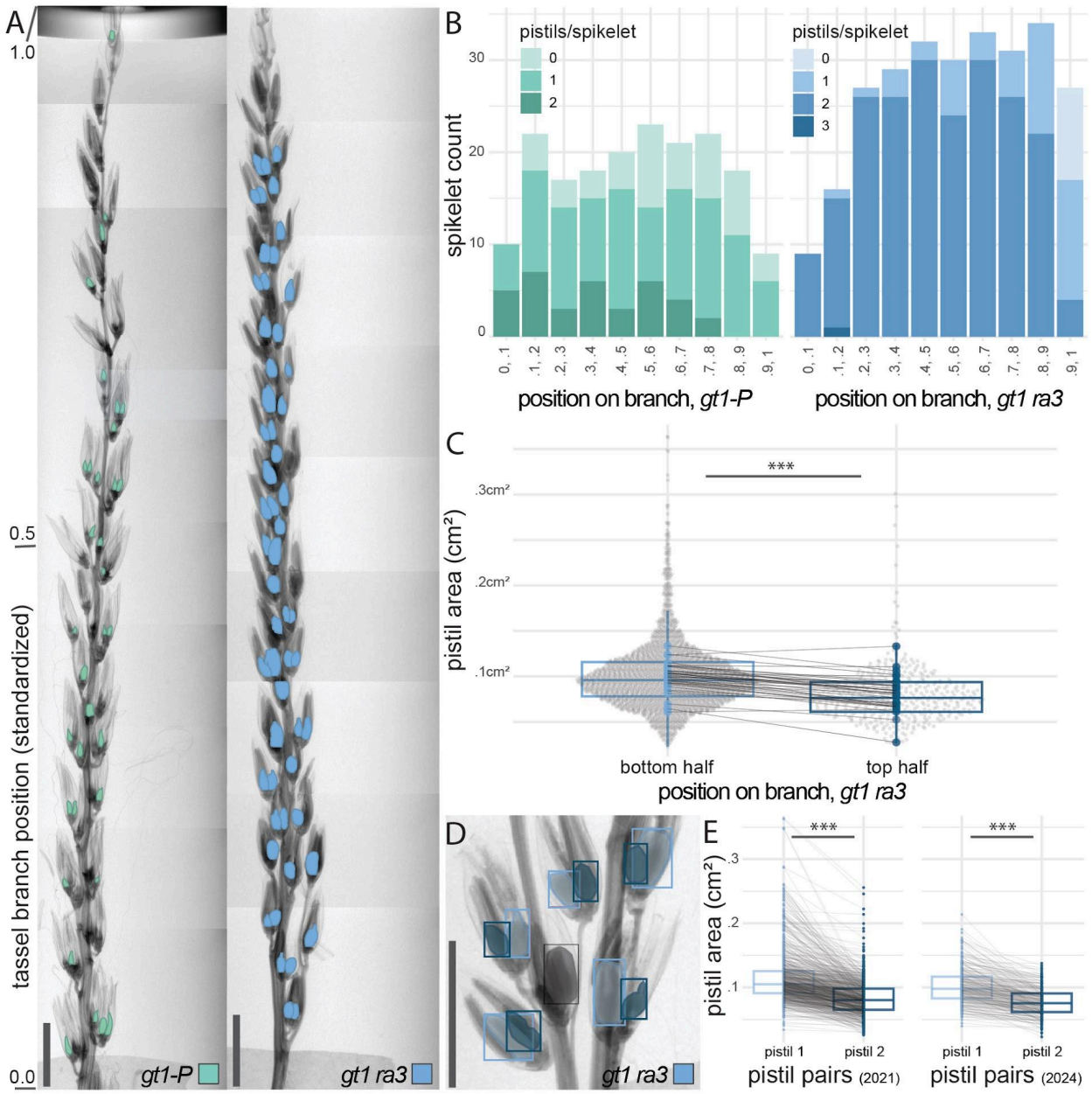

Figure 2. Pistil size changes by branch position. A) Examples of *gt1-P* and *gt1;ra3* tassel branch x-rays, showing pistil detection masks. The position of pistils on the tassel branch is standardized for each branch, with 0 being the base and 1.0 being the top. Scale bars = 1.9cm. B) Pistil presence/absence by tassel branch position. Pistils per spikelet for *gt1-P* and *gt1;ra3* plants. 5 plants measured per genotype (see Methods). C) Pistil area by tassel branch position. *gt1;ra3* tassel branches, bottom halves compared to top halves. Large dots represent the mean pistil area for the branch half, lines connect the same branch. Linear mixed model, pistil area ~ branch position (bottom/top) * block + (1 | plant). Estimated marginal means, $p < .05$, ***. D) Example of pistil spikelet pair detections - red, larger of pair; blue, smaller of pair; black, filtered (not part of a detection pair). E) *gt1;ra3* pistil pair size comparison within spikelets. Lines connect the pistil pairs, split by year. Student's t-test; $p < .05$, ***.

Because this method captures the outlines of pistils, we could also measure how shape changes across genotypes. We looked at various shape metrics, including elliptical fourier shape descriptors (Supplemental Fig. 1B) which revealed some previously unnoticed *gt1;ra3* and *tb1;gt1;ra3* phenotypes, including rare instances of triple pistils within one spikelet and pistils with abnormal morphology (Supplemental Fig. 1C). Upon closer inspection, the nucellus and an additional membrane (possibly an ovule integument) were overgrown and protruding out of the outer carpels, which were not fully fused (Supplemental Fig. 1D).

Defoliation affects pistil and branch suppression differently

We noticed that pistil size varies significantly across years (2021 *gt1;ra3* = 0.101 cm^2 ± 0.002; 2024 *gt1;ra3* = 0.091 cm^2 ± 0.002) (Fig 2C, E). Given that tillering is so sensitive to the environment (Tetio-Kagho and Gardner 1988; Doebley, Stec, and Gustus 1995), we wondered if different environmental conditions can affect pistil suppression. Since genes involved with environmental signalling are also involved in pistil growth suppression (Whipple et al. 2011), it's possible that pistil suppression in tassels is environmentally sensitive through similar mechanisms. To test this, we defoliated *gt1;ra3* plants during development, triggering sugar deprivation known to decrease tillering in maize (Kebrom, Brutnell, and Finlayson 2010; Kebrom and Mullet 2015).

If pistil suppression is sensitive to defoliation like tillering, we expect reduced pistil growth in tassels alongside reduced branching. We confirmed our defoliation treatment decreased tillering (no treatment = 1.08 ± 0.152; defoliated = 0.673 ± 0.128; n = 37) (Fig. 3B) and inflorescence branching (no treatment = 7.11 ± 0.62; defoliated = 5.06 ± 0.57; n = 37) (Fig. 3A), but it does not affect pistil size (no treatment = 0.100 cm^2 ± 0.001; defoliated = 0.098 cm^2 ± 0.002; tassel n = 37; no treatment pistil n = 2892; defoliated pistil n = 1558) (Fig. 3C) nor pistil shape (Supplemental Fig. 3). Instead, pistil size and shape stayed the same between treatments. Thus, pistils in *gt1;ra3* tassels are resilient to sugar deprivation under conditions that decrease the activity of other branching axes. One possibility is that *GT1* and *RA3* contribute more to environmentally mediated pistil suppression than in other axes, explaining the absence of a pistil phenotype in *gt1;ra3* mutants. Alternatively, it could also indicate that pistil and branch suppression respond differently to defoliation and that upstream regulation of suppression has diverged. In either case, these results indicate that suppression is controlled differently in pistils versus branches.

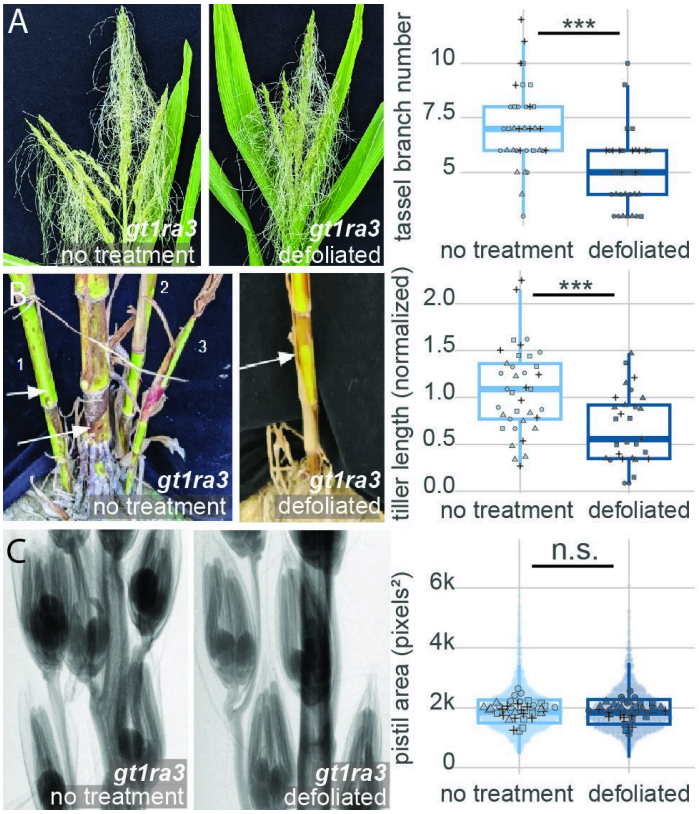

Figure 3. Defoliation affects tassel branch number and tiller length, but not pistil size. A) *gt1;ra3* tassels of untreated and defoliated plants. B) Bases of *gt1;ra3* plants, arrow indicates main stalk, numbers indicate tillers. Tassel branching and tillering significance tested with a 2-way ANOVA looking at block and treatment effect. *** = p-value < .05. C) Pistil x-rays from *gt1;ra3* tassels. Significance tested with a mixed linear model: pistil area ~ treatment * block + (1 | plant). n.s. = not significant.

The regulation of *GT1* by TB1 is distinct between tillers and pistils

In addition to sugar, light is a major regulator of tiller suppression, acting upstream of TEOSINTE BRANCHED1 (TB1) to promote tiller outgrowth in shade through differential regulation of its downstream target *GT1* (Tetio-Kagho and Gardner 1988; Kebrom, Burson, and Finlayson 2006; Whipple et al. 2011; Dong et al. 2019, 2017; Doebley, Stec, and Gustus 1995). The TCP family to which *TB1* belongs also has roles in floral suppression (Jiao et al. 2018; D. Luo et al. 1996; Yant et al. 2015), raising the possibility that *TB1* could contribute to pistil suppression, perhaps through a similar TB1-*GT1* pathway. However, pistil suppression appears normal in *tb1* single mutants, suggesting that other factors could be compensating for the loss of TB1 in this context. We therefore tested if *tb1* affects suppression in different sensitized mutant backgrounds, including the *tb1;gt1;ra3* triple.

We grew B73 (WT), *gt1-P*, *ra3*, *tb1*, *tb1;ra3* and *tb1;gt1;ra3* mutants in the field and x-rayed tassel branches for analysis (Fig. 4A). *tb1;gt1;ra3* mutants had tassel-like ear inflorescences with silks (Supplementary Fig. 4). After filtering out plants with tassels that had fewer than 5 detected pistils, only *gt1-P*, *gt1;ra3* and *tb1;gt1;ra3* plants remained. *gt1-P* pistils were smaller than both *gt1;ra3* and *tb1;gt1;ra3*; however *gt1;ra3* and *tb1;gt1;ra3* pistil sizes were not significantly different (Fig. 4B). *tb1*, *ra3* and *tb1;ra3* did not have visible pistils at maturity, as confirmed by SEM (Scanning Electron Microscopy) (Fig. 4C). Therefore, unlike other branching events, *tb1* does not affect pistil size in *ra3* and *gt1;ra3* backgrounds. The absence of pistils in *tb1;ra3* mutants, together with the finding that pistil size in *tb1;gt1;ra3* matches that of *gt1;ra3*, indicates that TB1 is unlikely to act upstream of *GT1* or *RA3* in tassel pistil suppression (Fig. 5).

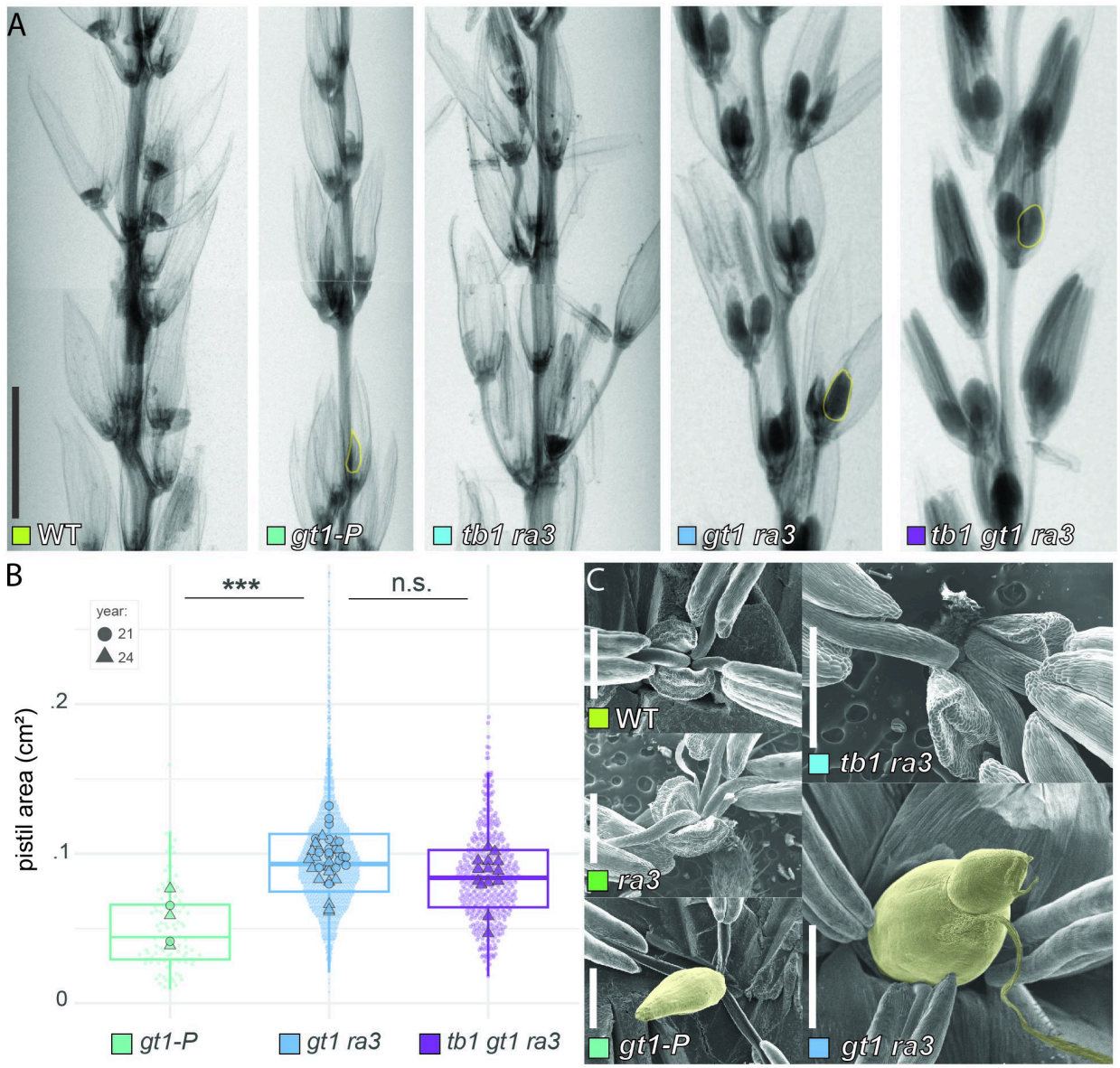

Figure 4. *tb1* does not significantly affect pistil size in *ra3* or *gt1;ra3* backgrounds. A) X-ray

tassel sections of WT (B73), *gt1-P*, *tb1;ra3*, *gt1;ra3*, and *tb1;gt1;ra3*. Example pistils are highlighted in yellow. B) Pistil area comparison between *gt1-P*, *gt1;ra3* and *tb1;gt1;ra3*. Additional plants were also included in this analysis (B73 - 9, *gt1-P* - 6, *tb1;ra3* - 2, *tb1* - 13, *ra3* - 2) however they all had less than 5 pistil detections per branch, which was considered the threshold for background noise, and were therefore filtered out. For statistical comparisons, a mixed linear model was used: pistil size ~ genotype * block + (1 | plant_id) with estimated marginal means. *** = $p < .05$; n.s. = not significant. C) SEM images of mature tassel florets from various genotypes. Pistils are highlighted with yellow.

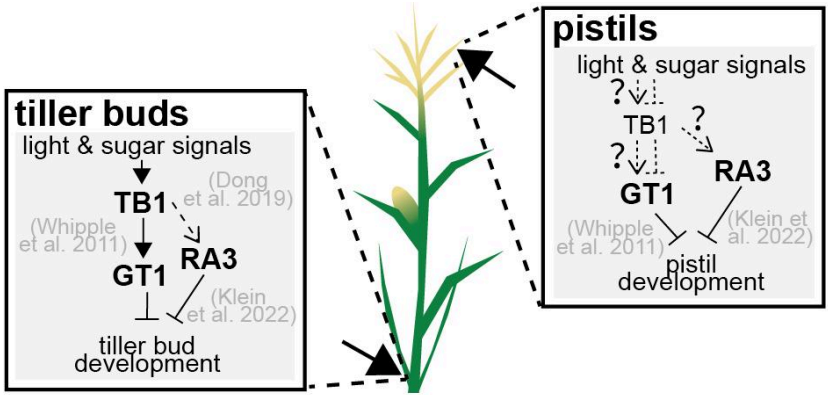

Figure 5. Models for suppression in tiller buds and pistils. Left) Tiller buds are suppressed by *GT1*, which is activated by TB1 in tiller buds in response to light and possibly sugar signals (Whipple et al. 2011; Mason et al. 2014). TB1 promotes the expression of *RA3* (Dong et al. 2019). RA3 suppresses tiller bud growth (Klein et al. 2022). Right) Possible model for pistil suppression. *ra3* and *gt1* mutations together have a synergistic effect on pistil growth, and *ra3* alone has a slight effect on pistil development (Klein et al. 2022). *gt1* mutants have derepressed tassel pistils (Whipple et al. 2011). It's unknown how light & sugar signals, as well as TB1, regulate *GT1* and *RA3* in pistils.

Discussion:

Some genes that suppress tiller growth in response to environmental cues are pleiotropic, and also suppress pistil growth (Whipple et al. 2011). To assess whether environmental factors influence floral development in maize, we developed a new method to precisely measure the size and shape of pistils in different conditions. Using this method, we found that defoliation, as a proxy for sugar deprivation (Kebrom, Brutnell, and Finlayson 2010; Kebrom and Mullet 2015) does not affect the size or shape of pistils in the tassel, even while it greatly reduces tillering and inflorescence branching. Through mutant comparisons, we determined that *GT1* is likely not downstream of TB1 in pistil suppression. These results suggest that tiller and pistil suppression mechanisms, while controlled by some of the same genes, have distinct upstream regulation.

Scientific progress is often limited by what one can see - observational gaps can create bottlenecks in understanding plant phenotypes (Atkinson et al. 2019). This especially applies to the study of pistil development in grasses, because pistils need to be individually dissected out of tiny spikelets to be measured. Floral development, specifically the formation of pistils vs. stamens in unisexual flowers, is quantitative rather than binary (Pannell 2017; Lloyd 1980), and the final form a flower takes can depend on several factors such as position (A. R. Orr et al. 2001; Diggle 1995), gene dosage (Moschin et al. 2021), and environment (Lan et al. 2023). These small quantitative differences in floral development are difficult to measure, especially in grasses. Our approach integrates x-ray imaging with machine learning-based segmentation, making it feasible to measure multiple pistils simultaneously, and extract detailed data regarding their size, shape, and position.

The ability to identify subtle phenotypic changes has broad application in biology, particularly in understanding complex plant traits and their evolution. The omnigenic model proposes that hundreds to thousands of genes influence a trait, but on their own genes may have very weak or no phenotype (Boyle, Li, and Pritchard 2017; Mähler et al. 2020). Complex dosage interactions amongst small-effect alleles may further modulate phenotypic outcomes (Zebell et al. 2025). Accurately identifying minor phenotypic differences can help detect small-effect alleles, and help reveal incremental genetic changes that underpin evolutionary processes and phenotypic diversity. Additionally, finding mutations that have weak effects on a trait can provide new variation for plant breeding programs (Rodríguez-Leal et al. 2017; Muños et al. 2011). While many new technologies can be expensive and inaccessible for many labs (Rogers et al. 2024), machine learning models are becoming increasingly accessible (Gehan et al. 2017; Winfree 2022). This work demonstrates how a fine-tuned computer vision model can be applied to a large image dataset to overcome phenotyping limitations and reveal new things about flower development.

Pleiotropy can be circumvented through cis-regulatory evolution (Carroll 2008). In contrast, our results suggest that pleiotropy might emerge when genes are redeployed across distinct developmental contexts, recruited by different upstream regulators. *GT1* is broadly capable of growth suppression, potentially through jasmonic acid signaling (Yuan et al. 2025; Klein et al. 2022). Supporting this generalizable function, ectopic expression of maize *GT1* in arabidopsis under a floral whorl-specific promoter reduced stamen and petal sizes (Gallagher et al. 2023)). Flexible regulatory mechanisms may allow unique roles for genes like *GT1* and *RA3* across developmental contexts, which then manifest as genetic pleiotropy in null mutants. In the grasses in particular, repeated recruitment of growth suppression genes may have led to floral diversification through the suppression of specific floral organs (Klein et al. 2022; Gallagher et al. 2023; Komatsuda et al. 2007)). In this case, recruitment of a growth suppression module may be a cause - not a consequence - of genetic pleiotropy.

Materials and Methods:

1. Plant Material and Growth Conditions

a. We used the maize genotypes B73, *gt1-P*, *ra3*, *tb1*, *tb1 ra3*, *gt1 ra3*, and *tb1 gt1 ra3* for phenotyping. We used the *gt1* allele *gt1-1* introgressed into B73 (Whipple et al. 2011; Klein et al. 2022). The *ra3* used was *ra3-fea1* (B73 background) (Satoh-Nagasawa et al. 2006). The *tb1* allele used was *tb1-ref* introgressed into B73 (Doebley, Stec, and Hubbard 1997). Maize was grown at the University of Massachusetts Amherst Crop and Animal Research and Education Farm in South Deerfield, MA (~42°290N, 72°350W) and setaria plants were grown at the College of Natural Sciences and Education Greenhouse on the UMass Amherst campus under long day conditions (16 h light, 8 h dark) at 28°C. Maize for defoliation experiments was grown at the University of Massachusetts Amherst Crop and Animal Research and Education Farm.

2. Defoliation Assay and Phenotyping
    a. Plants were split across different parts of the field in a block design. Every other plant in the row was defoliated by removing half of the most recently exposed leaf starting at 3 weeks after planting and repeating every 3-4 days for 5 weeks. This experiment was repeated for 2 field seasons. Tiller length measurements were standardized to plant height and then averaged per plant.
3. X-ray Imaging
    a. X-ray scans were captured using a Bruker Skyscan 1276 uCT at the Animal Imaging Core Facility on the UMass Amherst campus. Inflorescence samples were loaded horizontally into the machine. Samples were x-rayed from a reduced number of angles, and multiple scans were captured along the length of the sample. A single image angle from the top was selected and used in subsequent analyses. Scans were taken at 1008x672 resolution. The zoom level was set at 30µm per pixel for maize, and 40µm per pixel for setaria. All maize x-ray scans were taken at anthesis, and the bottommost tassel branch was used for imaging.
4. Pistil segmentation model
    a. Model Data Collection
        i. To train the model we first generated the training, validation and test data sets (Supplemental Table 1). Maize mutants with defects in tassel pistil repression were grown in either the field (UMass Amherst Crop and Animal Research and Education Farm) or the greenhouse (UMass Amherst College of Natural Sciences and Education Greenhouse). To obtain a range of pistil phenotypes, we grew the inbred line B73 as the negative control, *gt1-P*, *gt1 ra3* and *tb1 gt1 ra3* (hybrid background) mutants. We also included *Setaria viridis* inflorescence examples to make the model more generalizable for pistil detection in other grass species. For these examples, we collected setaria at various growth stages to get a range of pistil sizes for training. Setaria x-rays were collected at 4 developmental stages (28, 31, 33, 42 days after sowing (DAS)). Branches were removed from the setaria inflorescences with tweezers to reduce overlap, and the thinned inflorescence was used for imaging. After obtaining x-ray images for all samples, we annotated pistils by tracing using the Via-annotator program (Dutta and Zisserman 2019).

b. Model Data Preparation
    i. We used Roboflow (Dwyer, B., Nelson, J., Solawetz, J., et. al. 2022) to standardize the input image size in the case of different resolutions and to generate synthetic training examples using rotation (+- 10 degrees), brightness (+- 7%), and blur (up to .5px). The total dataset size was 332 tassel x-rays without synthetic data, and 664 after adding synthetic data. X-ray images were converted from tiff to jpg format, and pistil annotations were checked for accuracy in a Jupyter notebook (available on Github) before training.
c. Model Selection and Training
    i. Pistils in x-ray images are dense (20+ pistils per image) and overlapping. Because of this, Mask-RCNN (He et al. 2017) was chosen as the base model due to its ability to segment overlapping objects effectively (Rettenberger et al. 2023). Pistil-specific models were trained using Mask R-CNN with a ResNet-101-FPN backbone, pretrained on ImageNet and obtained from the Detectron2 Model Zoo (Yuxin Wu, Alexander Kirillov, Francisco Massa, Wan-Yen Lo, Ross Girshick 2019). Models were trained using the Detectron2 framework using the default Mask-RCNN hyperparameter configurations. Training was completed on the Unity Cluster located at the Massachusetts Green High Performance Computing Center. During training several metrics were logged every 200 iterations, including total loss, validation loss, bounding box AP and segmentation AP. Model selection was based on the lowest validation loss. Checkpoints were saved every 200 iterations, and the final model was selected at iteration 1399 when validation loss plateaued.
d. Model Evaluation
    i. We used stratified 5-fold cross-validation to evaluate model performance (Supplemental Table 2). Data splitting was implemented in Python using StratifiedKFold from scikit-learn, stratified by plant species (maize vs. setaria) and pistil size category (small, medium, large, extra-large). This ensured each fold contained a balanced composition of image types. For each fold, models were trained as described above, and training was stopped at 1399 iterations. Model performance across folds was assessed using bounding box and segmentation precision (AP) and consistency was compared across splits.
    ii. The final model was evaluated using the hold-out test set with coco evaluation metrics (Supplemental Table 3). Lastly, a confidence threshold of 0.82 was applied to maximize the F1 score at high IoUs (Supplemental Figure 1).

5. Pistil area and shape genotype comparison
    a. Maize plants from all genotypes were grown for pistil area and shape quantification (see Plant Material and Growth Conditions). Tassel x-ray scans were collected as described above. The final pistil segmentation model with the 0.82 confidence threshold applied was used to generate pistil masks from the

x-ray scans. First, pistil detections were filtered to remove detections of cut-off pistils at the edges of the image. Duplicate pistils in the regions where successive x-ray scans overlap were also removed. Tassels with less than 5 detections per tassel were filtered from the analysis. Pistil size was calculated from the total pixels in the detection mask. Pistil shape metrics were calculated using Python OpenCV. Fourier shape analysis was done using the program SHAPE (Iwata and Ukai 2002).

b. To quantify the pistil presence/absence by tassel branch position, model outputs were manually checked against the original x-rays to ensure no pistil detections were missed. To find pistil pairs within spikelets, a custom python script was used to identify instances where only two pistil masks overlapped. Any singletons or overlaps of more than two pistils were discarded from the analysis. Identified pistil pairs were viewed to confirm pairs were correct before downstream analysis.

c. All analysis was done in Jupyter notebooks or R, and files are available on Github.

6. Genotyping Assays
   a. *tb1 ra3* and *tb1 gt1 ra3* plants were genotyped with the following primers:*tb1-ref* forward - GCCTTGGAGTCCCATCAGT, *tb1-ref* reverse - TTCATCGTCACACAGCCAAT; *ra3-fea1* forward CGGGAGGCGGGGAACTAATA, *ra3-fea1* reverse - AGTAGCACTCTGGGAAAGCG.
7. Scanning Electron Microscopy (SEM)
   b. SEM was performed with a JEOL JCM-6000 Plus Neoscope Benchtop scanning electron microscope with fresh tissue samples. Late-stage florets were dissected from the tassel and transferred to the SEM. Images were recorded under high vacuum and 5-kV voltage within 15 min of being in the SEM.

Supplemental Figures and Tables

Figures:

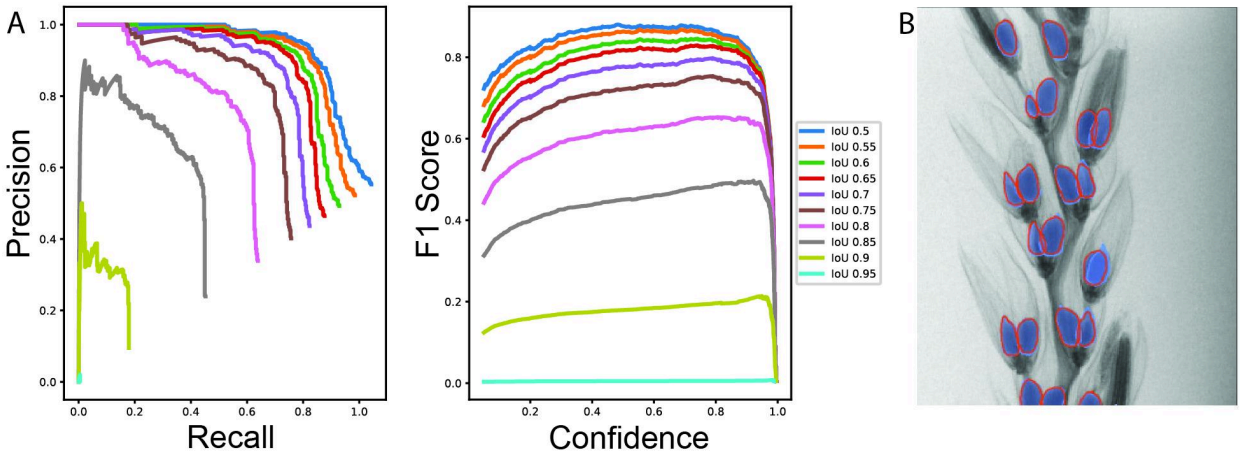

C

IoU Mean / Median / Mode	Precision - AP50	Precision - AP75	Precision - mAP
.79, .83, .85	.96	.83	.70
IoU Variance	**Recall - AR50**	**Recall - AR75**	**Recall - mAR**
Q1: .73, Q2: .79, Q3: .89, IQR: .15	.77	.67	.56

Supplemental Figure 1: **Model Performance Summary @ 0.82 Confidence Threshold.** A) Precision vs. Recall curves for final model performance on hold-out test dataset, split by IoU threshold. F1 Score vs. Confidence for final model performance on hold-out test dataset, split by IoU threshold. For this application we prioritized segmentation accuracy and precision over recall. The maximum F1 scores at high IoU thresholds occurred at or above 0.82, so we used 0.82 as the confidence threshold. B) Example detections (red outlines) and ground truth (blue shading) of a *gt1 ra3* maize plant at the 0.82 confidence threshold. C) Final model performance statistics at the 0.82 confidence threshold used for analysis. Segmentation precision and recall are reported at the .50 IoU threshold (AP50, AR50) and .75 IoU threshold (AP75, AR75). The mean average precision and recall (mAP, mAR) are calculated by taking the mean of the APs/ARs from the .50 to .95 IoU thresholds, in steps of .05.

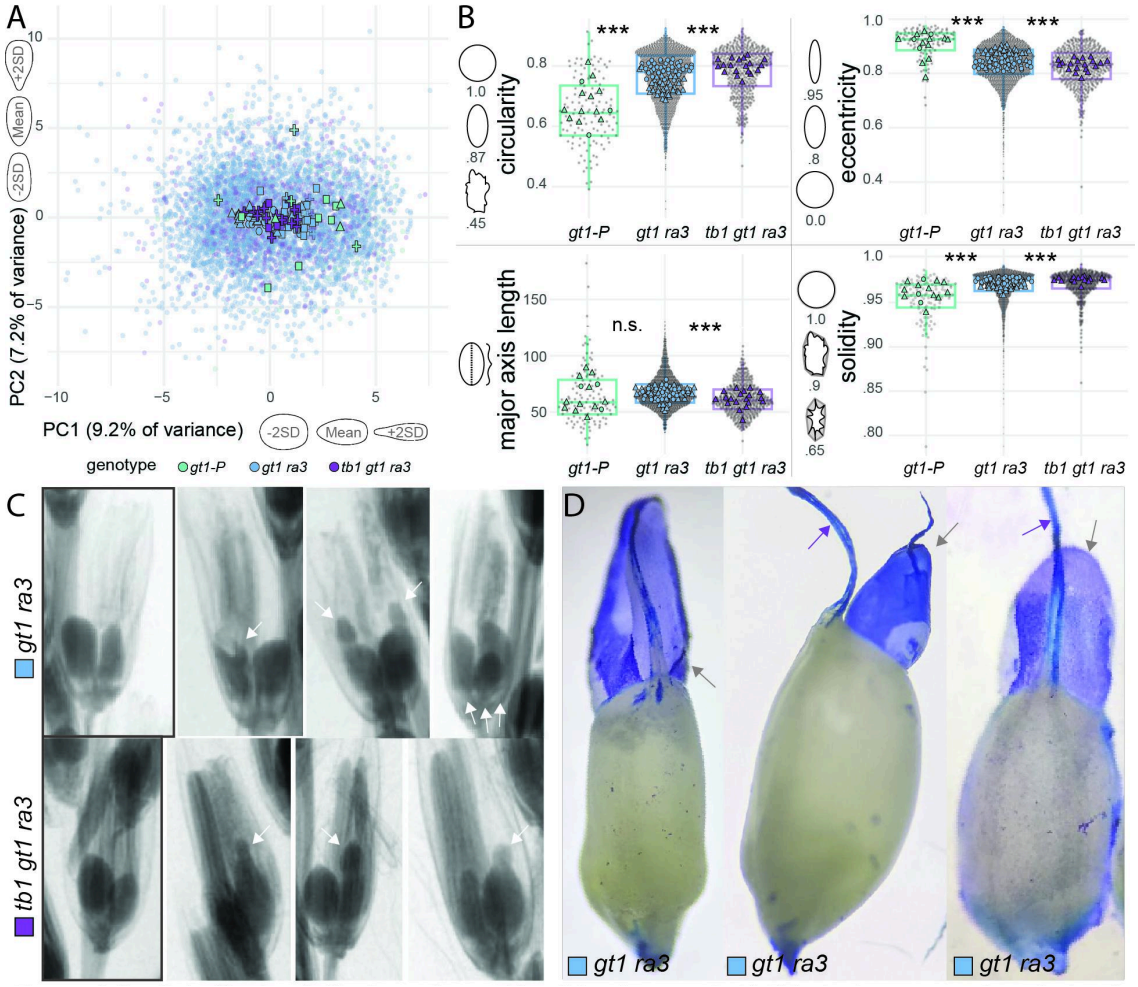

Supplemental Figure 2. Pistil shape varies across genotypes. A) Principal component analysis of elliptical Fourier pistil descriptors. Large shapes on the graph show the mean value of all pistils per tassel. B) Shape metric comparison with example shapes on the left. Genotype statistical comparisons were done with a mixed linear model: shape metric ~ genotype * block + (1 | plant) and estimated marginal means. *** = p-value < .05, n.s. = not significant. C) Examples of pistils from x-rays. Pistils with normal morphology are on the left. Pistils to the right are abnormal, with arrows indicating excess tissue. The last *gt1;ra3* spikelet shows three pistils instead of two. D) Dissected abnormal *gt1;ra3* pistils, stained with toluidine blue. Grey arrows indicate possible integument overgrowth, which is stained more darkly than the underlying nucellus. Purple arrows indicate silks.

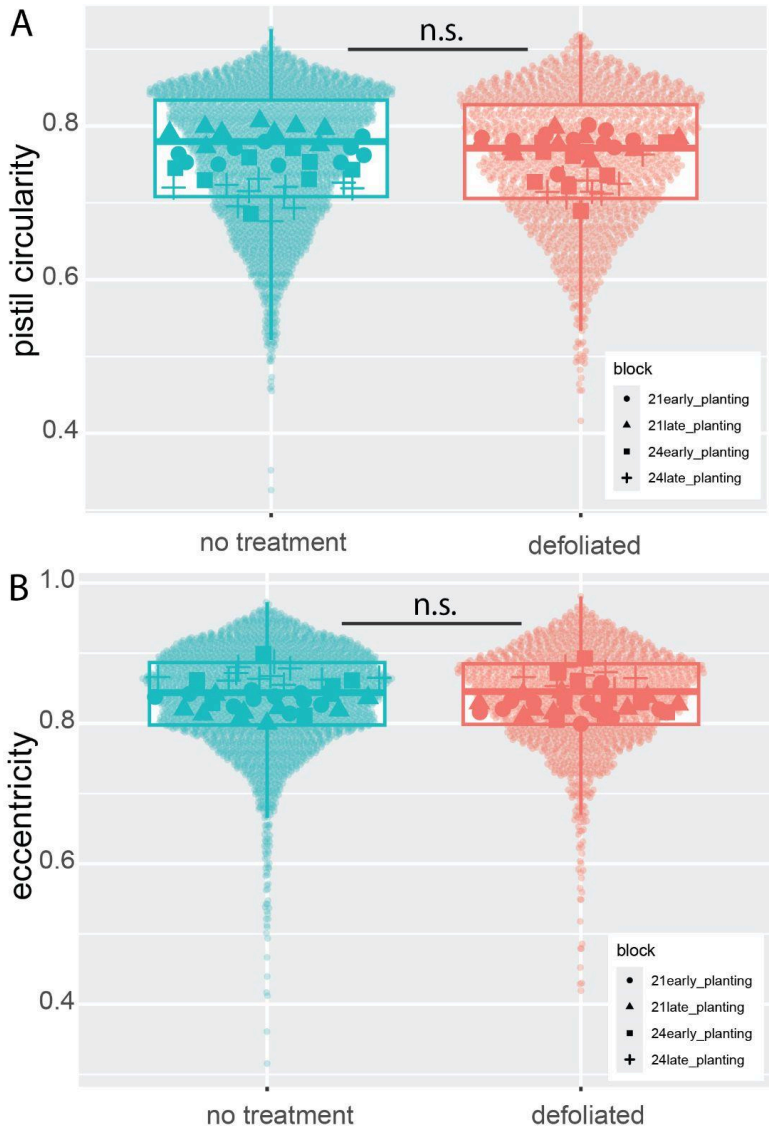

Supplemental Figure 3. Defoliation of *gt1 ra3* plants does not affect pistil shape. A) Pistil circularity compared between treatments. Large shapes show the average for each tassel. Significance test: Linear mixed model, circularity ~ treatment * block * (1 | plant). B) Pistil eccentricity compared between treatments. Significance test: Linear mixed model, eccentricity ~ treatment * block * (1 | plant)

A
tb1 gt1 ra3
B
tb1 gt1 ra3
C
tb1
tb1
D
tb1 gt1 ra3
tb1 gt1 ra3

Supplemental Figure 4. *tb1 gt1 ra3* phenotypes. A) *tb1 gt1 ra3* whole plant, showing tillering. B) Close up of *tb1 gt1 ra3* middle section. White arrows show tiller-like structures in place of ears. C) A *tb1* tiller in place of an ear. D) A *tb1 gt1 ra3* tiller in place of an ear, arrow shows the silks of the derepressed carpels.

Tables:

species	pistil size	genotype	stage	training images	validation images	test images
Zea mays	none	B73 (WT)	anthesis	0	3	3
Zea mays	none-small	*gt1-P*	anthesis	33	8	7
Zea mays	medium	*gt1 ra3*	anthesis	64	12	11
Zea mays	large	*tb1 gt1 ra3* (hybrid)	anthesis	16	4	4
Setaria viridis	none-small	A10.1 (WT)	21 DAS	29	7	6
Setaria viridis	none-small	*svra3-1*				
Setaria viridis	medium	A10.1 (WT)	31 DAS	32	6	6
Setaria viridis	medium	*svra3-1*				
Setaria viridis	large	A10.1 (WT)	33 DAS	30	6	6
Setaria viridis	large	*svra3-1*				
Setaria viridis	XL	A10.1 (WT)	42 DAS	27	6	6
Setaria viridis	XL	*svra3-1*				

Supplemental Table 1: Overview of training, validation, and test datasets for model

	bbox AP50	**bbox AP75**	**bbox mAP**	**segm AP50**	**segm AP75**	**segm mAP**
Fold 0	81.6	47.3	45.7	81.9	55.0	49.5
Fold 1	83.1	51.4	47.8	82.8	55.5	50.2
Fold 2	82.4	50.3	47.2	82.3	56.2	49.7
Fold 3	83.1	52.0	48.1	83.3	55.6	50.1
Fold 4	81.0	48.0	46.3	81.0	52.7	48.0
Mean ± SD	82.2 ± 0.9	49.8 ± 2.1	47.0 ± 1.0	82.3 ± 0.9	55.0 ± 1.4	49.5 ± 0.9

Supplemental Table 2: 5-Fold stratified cross validation. bbox = bounding box, segm = segmentation.

	bbox AP50	**bbox AP75**	**bbox mAP**	**segm AP50**	**segm AP75**	**segm mAP**
Final model	87.3	61.9	54.1	86.9	64.7	56.7

Supplemental Table 3: Model performance on hold-out test set, no confidence threshold applied. bbox = bounding box, segm = segmentation.

Acknowledgements: Dan Chitwood, Clint Whipple, Elizabeth Kellogg, Anna Green, Isabella Higgins, Anna Liu & UMass Statistical Consulting group, UMass HPCC staff, UMass Greenhouse staff

References:

Aguilar-Martínez, José Antonio, César Poza-Carrión, and Pilar Cubas. 2007. “Arabidopsis BRANCHED1 Acts as an Integrator of Branching Signals within Axillary Buds.” *The Plant Cell* 19 (2): 458–72.

Atkinson, Jonathan A., Michael P. Pound, Malcolm J. Bennett, and Darren M. Wells. 2019. “Uncovering the Hidden Half of Plants Using New Advances in Root Phenotyping.” *Current Opinion in Biotechnology* 55 (February):1–8.

Barbier, François F., John E. Lunn, and Christine A. Beveridge. 2015. “Ready, Steady, Go! A Sugar Hit Starts the Race to Shoot Branching.” *Current Opinion in Plant Biology* 25 (June):39–45.

Barbier, François, Thomas Péron, Marion Lecerf, Maria-Dolores Perez-Garcia, Quentin Barrière, Jakub Rolčík, Stéphanie Boutet-Mercey, et al. 2015. “Sucrose Is an Early Modulator of the Key Hormonal Mechanisms Controlling Bud Outgrowth in Rosa Hybrida.” *Journal of Experimental Botany* 66 (9): 2569–82.

Bertolini, Edoardo, Brian R. Rice, Max Braud, Jiani Yang, Sarah Hake, Josh Strable, Alexander E. Lipka, and Andrea L. Eveland. 2025. “Regulatory Variation Controlling Architectural Pleiotropy in Maize.” *Nature Communications* 16 (1): 2140.

Boyle, Evan A., Yang I. Li, and Jonathan K. Pritchard. 2017. “An Expanded View of Complex Traits: From Polygenic to Omnigenic.” *Cell* 169 (7): 1177–86.

Calderon-Urrea, A., and S. L. Dellaporta. 1999. “Cell Death and Cell Protection Genes Determine the Fate of Pistils in Maize.” *Development* 126 (3): 435–41.

Carroll, Sean B. 2005. “Evolution at Two Levels: On Genes and Form.” *PLoS Biology* 3 (7): e245.

———. 2008. “Evo-Devo and an Expanding Evolutionary Synthesis: A Genetic Theory of Morphological Evolution.” *Cell* 134 (1): 25–36.

Demotes-Mainard, Sabine, Thomas Péron, Adrien Corot, Jessica Bertheloot, José Le Gourrierec, Sandrine Pelleschi-Travier, Laurent Crespel, et al. 2016. “Plant Responses to

Red and Far-Red Lights, Applications in Horticulture." *Environmental and Experimental Botany* 121 (January):4–21.
Diggle, P. 1995. "Architectural Effects and the Interpretation of Patterns of Fruit and Seed Development." *Annual Review of Ecology, Evolution, and Systematics* 26:531–52.
Dixon, Laura E., Julian R. Greenwood, Stefano Bencivenga, Peng Zhang, James Cockram, Gregory Mellers, Kerrie Ramm, Colin Cavanagh, Steve M. Swain, and Scott A. Boden. 2018. "TEOSINTE BRANCHED1 Regulates Inflorescence Architecture and Development in Bread Wheat (Triticum Aestivum)." *The Plant Cell* 30 (3): 563–81.
Doebley, J., A. Stec, and C. Gustus. 1995. "Teosinte branched1 and the Origin of Maize: Evidence for Epistasis and the Evolution of Dominance." *Genetics* 141 (1): 333–46.
Doebley, J., A. Stec, and L. Hubbard. 1997. "The Evolution of Apical Dominance in Maize." *Nature* 386 (6624): 485–88.
Dong, Zhaobin, Wei Li, Erica Unger-Wallace, Jinliang Yang, Erik Vollbrecht, and George Chuck. 2017. "Ideal Crop Plant Architecture Is Mediated by Tassels Replace Upper ears1, a BTB/POZ Ankyrin Repeat Gene Directly Targeted by TEOSINTE BRANCHED1." *Proceedings of the National Academy of Sciences of the United States of America* 114 (41): E8656–64.
Dong, Zhaobin, Yuguo Xiao, Rajanikanth Govindarajulu, Regina Feil, Muriel L. Siddoway, Torrey Nielsen, John E. Lunn, Jennifer Hawkins, Clinton Whipple, and George Chuck. 2019. "The Regulatory Landscape of a Core Maize Domestication Module Controlling Bud Dormancy and Growth Repression." *Nature Communications* 10 (1): 3810.
Dutta, Abhishek, and Andrew Zisserman. 2019. "The VIA Annotation Software for Images, Audio and Video." *arXiv [cs.CV]*. arXiv. http://arxiv.org/abs/1904.10699.
Dwyer, B., Nelson, J., Solawetz, J., et. al. 2022. "Roboflow (Version 1.0) [Software]." 2022. https://roboflow.com.
Egger, Rachel L., and Virginia Walbot. 2015. "Quantifying Zea Mays L Tassel Development and Correlation with Anther Developmental Stages as a Guide for Experimental Studies." 2015. https://core.ac.uk/download/pdf/230662358.pdf.
Fichtner, Franziska, Francois F. Barbier, Maria G. Annunziata, Regina Feil, Justyna J. Olas, Bernd Mueller-Roeber, Mark Stitt, Christine A. Beveridge, and John E. Lunn. 2021. "Regulation of Shoot Branching in Arabidopsis by Trehalose 6-Phosphate." *The New Phytologist* 229 (4): 2135–51.
Fichtner, Franziska, Francois F. Barbier, Regina Feil, Mutsumi Watanabe, Maria Grazia Annunziata, Tinashe G. Chabikwa, Rainer Höfgen, Mark Stitt, Christine A. Beveridge, and John E. Lunn. 2017. "Trehalose 6-Phosphate Is Involved in Triggering Axillary Bud Outgrowth in Garden Pea (Pisum Sativum L.)." *The Plant Journal: For Cell and Molecular Biology* 92 (4): 611–23.
Foster, Kevin R., Gad Shaulsky, Joan E. Strassmann, David C. Queller, and Chris R. L. Thompson. 2004. "Pleiotropy as a Mechanism to Stabilize Cooperation." *Nature* 431 (7009): 693–96.
Gallagher, Joseph P., Jarrett Man, Adriana Chiaramida, Isabella K. Rozza, Erin L. Patterson, Morgan M. Powell, Amanda Schrager-Lavelle, Dilbag S. Multani, Robert B. Meeley, and Madelaine E. Bartlett. 2023. "*GRASSY TILLERS1* (*GT1*) and *SIX-ROWED SPIKE1* (*VRS1*) Homologs Share Conserved Roles in Growth Repression." *Proceedings of the National Academy of Sciences of the United States of America* 120 (51): e2311961120.
Gehan, Malia A., Noah Fahlgren, Arash Abbasi, Jeffrey C. Berry, Steven T. Callen, Leonardo Chavez, Andrew N. Doust, et al. 2017. "PlantCV v2: Image Analysis Software for High-Throughput Plant Phenotyping." *PeerJ* 5 (December):e4088.
González-Grandío, Eduardo, Alice Pajoro, José M. Franco-Zorrilla, Carlos Tarancón, Richard G. H. Immink, and Pilar Cubas. 2017. "Abscisic Acid Signaling Is Controlled by a BRANCHED1/HD-ZIP I Cascade in Arabidopsis Axillary Buds." *Proceedings of the National*

Academy of Sciences of the United States of America 114 (2): E245–54.
González-Grandío, Eduardo, César Poza-Carrión, Carlos Oscar S. Sorzano, and Pilar Cubas. 2013. “BRANCHED1 Promotes Axillary Bud Dormancy in Response to Shade in Arabidopsis.” *The Plant Cell* 25 (3): 834–50.
Hämälä, Tuomas, Amanda J. Gorton, David A. Moeller, and Peter Tiffin. 2020. “Pleiotropy Facilitates Local Adaptation to Distant Optima in Common Ragweed (Ambrosia Artemisiifolia).” *PLoS Genetics* 16 (3): e1008707.
He, Kaiming, Georgia Gkioxari, Piotr Dollár, and Ross Girshick. 2017. “Mask R-CNN.” *arXiv [cs.CV]*. arXiv. http://arxiv.org/abs/1703.06870.
Iwata, H., and Y. Ukai. 2002. “SHAPE: A Computer Program Package for Quantitative Evaluation of Biological Shapes Based on Elliptic Fourier Descriptors.” *The Journal of Heredity* 93 (5): 384–85.
Jiao, Yinping, Young Koung Lee, Nicholas Gladman, Ratan Chopra, Shawn A. Christensen, Michael Regulski, Gloria Burow, et al. 2018. “MSD1 Regulates Pedicellate Spikelet Fertility in Sorghum through the Jasmonic Acid Pathway.” *Nature Communications* 9 (1): 822.
Johnston, Robyn, Minghui Wang, Qi Sun, Anne W. Sylvester, Sarah Hake, and Michael J. Scanlon. 2014. “Transcriptomic Analyses Indicate That Maize Ligule Development Recapitulates Gene Expression Patterns That Occur during Lateral Organ Initiation.” *The Plant Cell* 26 (12): 4718–32.
Kebrom, Tesfamichael H., Thomas P. Brutnell, and Scott A. Finlayson. 2010. “Suppression of Sorghum Axillary Bud Outgrowth by Shade, phyB and Defoliation Signalling Pathways.” *Plant, Cell & Environment* 33 (1): 48–58.
Kebrom, Tesfamichael H., Byron L. Burson, and Scott A. Finlayson. 2006. “Phytochrome B Represses Teosinte Branched1 Expression and Induces Sorghum Axillary Bud Outgrowth in Response to Light Signals.” *Plant Physiology* 140 (3): 1109–17.
Kebrom, Tesfamichael H., and John E. Mullet. 2015. “Photosynthetic Leaf Area Modulates Tiller Bud Outgrowth in Sorghum.” *Plant, Cell & Environment* 38 (8): 1471–78.
King, M. C., and A. C. Wilson. 1975. “Evolution at Two Levels in Humans and Chimpanzees: Their Macromolecules Are so Alike That Regulatory Mutations May Account for Their Biological Differences.” *Science (New York, N.Y.)* 188 (4184): 107–16.
Klein, Harry, Joseph Gallagher, Edgar Demesa-Arevalo, María Jazmín Abraham-Juárez, Michelle Heeney, Regina Feil, John E. Lunn, et al. 2022. “Recruitment of an Ancient Branching Program to Suppress Carpel Development in Maize Flowers.” *Proceedings of the National Academy of Sciences of the United States of America* 119 (2). https://doi.org/10.1073/pnas.2115871119.
Komatsuda, Takao, Mohammad Pourkheirandish, Congfen He, Perumal Azhaguvel, Hiroyuki Kanamori, Dragan Perovic, Nils Stein, et al. 2007. “Six-Rowed Barley Originated from a Mutation in a Homeodomain-Leucine Zipper I-Class Homeobox Gene.” *Proceedings of the National Academy of Sciences of the United States of America* 104 (4): 1424–29.
Kostyun, Jamie L., Matthew J. S. Gibson, Christian M. King, and Leonie C. Moyle. 2019. “A Simple Genetic Architecture and Low Constraint Allow Rapid Floral Evolution in a Diverse and Recently Radiating Plant Genus.” *The New Phytologist* 223 (2): 1009–22.
Kumar, Vikranth, Sung Hoon Kim, Moch Rosyadi Adnan, Jung Heo, Jin Hee Jeong, Ryza A. Priatama, Jeung Joo Lee, et al. 2021. “Tiller Outgrowth in Rice (Oryza Sativa L.) Is Controlled by OsGT1, Which Acts Downstream of FC1 in a PhyB-Independent Manner.” *Journal of Plant Biology* 64 (5): 417–30.
Lan, Jingqiu, Ning Wang, Yutao Wang, Yidan Jiang, Hao Yu, Xiaofeng Cao, and Genji Qin. 2023. “Arabidopsis TCP4 Transcription Factor Inhibits High Temperature-Induced Homeotic Conversion of Ovules.” *Nature Communications* 14 (1): 5673.
Le Roux, L. G., and E. A. Kellogg. 1999. “Floral Development and the Formation of Unisexual Spikelets in the Andropogoneae (Poaceae).” *American Journal of Botany* 86 (3): 354–66.

Lloyd, David G. 1980. “The Distributions of Gender in Four Angiosperm Species Illustrating Two Evolutionary Pathways to Dioecy.” *Evolution; International Journal of Organic Evolution* 34 (1): 123.
Luo, D., R. Carpenter, C. Vincent, L. Copsey, and E. Coen. 1996. “Origin of Floral Asymmetry in Antirrhinum.” *Nature* 383 (6603): 794–99.
Luo, Zhiwei, Bart J. Janssen, and Kimberley C. Snowden. 2021. “The Molecular and Genetic Regulation of Shoot Branching.” *Plant Physiology* 187 (3): 1033–44.
Mähler, Niklas, Bastian Schiffthaler, Kathryn M. Robinson, Barbara K. Terebieniec, Matej Vučak, Chanaka Mannapperuma, Mark E. S. Bailey, Stefan Jansson, Torgeir R. Hvidsten, and Nathaniel R. Street. 2020. “Leaf Shape in Populus Tremula Is a Complex, Omnigenic Trait.” *Ecology and Evolution* 10 (21): 11922–40.
Martín-Trillo, Mar, Eduardo González Grandío, François Serra, Fabien Marcel, María Luisa Rodríguez-Buey, Gregor Schmitz, Klaus Theres, Abdelhafid Bendahmane, Hernán Dopazo, and Pilar Cubas. 2011. “Role of Tomato BRANCHED1-like Genes in the Control of Shoot Branching: A BRC1-like Gene Controls Shoot Branching in Tomato.” *The Plant Journal: For Cell and Molecular Biology* 67 (4): 701–14.
Mason, Michael G., John J. Ross, Benjamin A. Babst, Brittany N. Wienclaw, and Christine A. Beveridge. 2014. “Sugar Demand, Not Auxin, Is the Initial Regulator of Apical Dominance.” *Proceedings of the National Academy of Sciences of the United States of America* 111 (16): 6092–97.
Moschin, Silvia, Sebastiano Nigris, Ignacio Ezquer, Simona Masiero, Stefano Cagnin, Enrico Cortese, Lucia Colombo, Giorgio Casadoro, and Barbara Baldan. 2021. “Expression and Functional Analyses of Nymphaea Caerulea MADS-Box Genes Contribute to Clarify the Complex Flower Patterning of Water Lilies.” *Frontiers in Plant Science* 12 (September):730270.
Muños, Stéphane, Nicolas Ranc, Emmanuel Botton, Aurélie Bérard, Sophie Rolland, Philippe Duffé, Yolande Carretero, et al. 2011. “Increase in Tomato Locule Number Is Controlled by Two Single-Nucleotide Polymorphisms Located near WUSCHEL.” *Plant Physiology* 156 (4): 2244–54.
Nuccio, Michael L., Jeff Wu, Ron Mowers, Hua-Ping Zhou, Moez Meghji, Lucia F. Primavesi, Matthew J. Paul, et al. 2015. “Expression of Trehalose-6-Phosphate Phosphatase in Maize Ears Improves Yield in Well-Watered and Drought Conditions.” *Nature Biotechnology* 33 (8): 862–69.
Orr, A. R., R. Kaparthi, C. L. Dewald, and M. D. Sundberg. 2001. “Analysis of Inflorescence Organogenesis in Eastern Gamagrass, Tripsacum Dactyloides (Poaceae): The Wild Type and the Gynomonoecious gsf1 Mutant.” *American Journal of Botany* 88 (3): 363–81.
Orr, H. A. 2000. “Adaptation and the Cost of Complexity.” *Evolution; International Journal of Organic Evolution* 54 (1): 13–20.
Pannell, John R. 2017. “Plant Sex Determination.” *Current Biology: CB* 27 (5): R191–97.
Patil, Suyash B., Francois F. Barbier, Jinfeng Zhao, Syed A. Zafar, Muhammad Uzair, Yinglu Sun, Jingjing Fang, et al. 2022. “Sucrose Promotes D53 Accumulation and Tillering in Rice.” *The New Phytologist* 234 (1): 122–36.
Prud’homme, Benjamin, Nicolas Gompel, and Sean B. Carroll. 2007. “Emerging Principles of Regulatory Evolution.” *Proceedings of the National Academy of Sciences of the United States of America* 104 Suppl 1 (suppl_1): 8605–12.
Qian, Dong, Muxuan Wang, Yue Niu, Yang Yang, and Yun Xiang. 2025. “Sexual Reproduction in Plants under High Temperature and Drought Stress.” *Cell Reports* 44 (3): 115390.
Rainio, Oona, Jarmo Teuho, and Riku Klén. 2024. “Evaluation Metrics and Statistical Tests for Machine Learning.” *Scientific Reports* 14 (1): 6086.
Rameau, Catherine, Jessica Bertheloot, Nathalie Leduc, Bruno Andrieu, Fabrice Foucher, and Soulaiman Sakr. 2014. “Multiple Pathways Regulate Shoot Branching.” *Frontiers in Plant*

Science 5:741.
Rettenberger, Luca, Friedrich Rieken Münke, Roman Bruch, and Markus Reischl. 2023. “Mask R-CNN Outperforms U-Net in Instance Segmentation for Overlapping Cells.” *Current Directions in Biomedical Engineering* 9 (1): 335–38.
Rodríguez-Leal, Daniel, Zachary H. Lemmon, Jarrett Man, Madelaine E. Bartlett, and Zachary B. Lippman. 2017. “Engineering Quantitative Trait Variation for Crop Improvement by Genome Editing.” *Cell* 171 (2): 470–80.e8.
Rogers, Crystal D., Chris Amemiya, Swathi Arur, Leslie Babonis, Michael Barresi, Madelaine Bartlett, Richard Behringer, et al. 2024. “Pluripotency of a Founding Field: Rebranding Developmental Biology.” *Development (Cambridge, England)* 151 (3): dev202342.
Sánchez-Gerschon, Verónica, Irene Martínez-Fernández, María R. González-Bermúdez, Sergio de la Hoz-Rodríguez, Florenci V. González, Jorge Lozano-Juste, Cristina Ferrándiz, and Vicente Balanzà. 2024. “Transcription Factors HB21/40/53 Trigger Inflorescence Arrest through Abscisic Acid Accumulation at the End of Flowering.” *Plant Physiology* 195 (4): 2743–56.
Satoh-Nagasawa, Namiko, Nobuhiro Nagasawa, Simon Malcomber, Hajime Sakai, and David Jackson. 2006. “A Trehalose Metabolic Enzyme Controls Inflorescence Architecture in Maize.” *Nature* 441 (7090): 227–30.
Stearns, Frank W. 2010. “One Hundred Years of Pleiotropy: A Retrospective.” *Genetics* 186 (3): 767–73.
Takeda, Taito, Yuko Suwa, Makoto Suzuki, Hidemi Kitano, Miyako Ueguchi-Tanaka, Motoyuki Ashikari, Makoto Matsuoka, and Chiharu Ueguchi. 2003. “The OsTB1 Gene Negatively Regulates Lateral Branching in Rice.” *The Plant Journal: For Cell and Molecular Biology* 33 (3): 513–20.
Tetio-Kagho, F., and F. P. Gardner. 1988. “Responses of Maize to Plant Population Density. I. Canopy Development, Light Relationships, and Vegetative Growth.” *Agronomy Journal* 80 (6): 930–35.
Welch, John J., and David Waxman. 2003. “Modularity and the Cost of Complexity.” *Evolution; International Journal of Organic Evolution* 57 (8): 1723–34.
Whipple, Clinton J., Tesfamichael H. Kebrom, Allison L. Weber, Fang Yang, Darren Hall, Robert Meeley, Robert Schmidt, John Doebley, Thomas P. Brutnell, and David P. Jackson. 2011. “Grassy tillers1 Promotes Apical Dominance in Maize and Responds to Shade Signals in the Grasses.” *Proceedings of the National Academy of Sciences of the United States of America* 108 (33): E506–12.
Winfree, Seth. 2022. “User-Accessible Machine Learning Approaches for Cell Segmentation and Analysis in Tissue.” *Frontiers in Physiology* 13 (March):833333.
Yang, Hailong, Kate Nukunya, Queying Ding, and Beth E. Thompson. 2022. “Tissue-Specific Transcriptomics Reveal Functional Differences in Floral Development.” *Plant Physiology* 188 (2): 1158–73.
Yant, Levi, Silvio Collani, Joshua Puzey, Clara Levy, and Elena M. Kramer. 2015. “Molecular Basis for Three-Dimensional Elaboration of the Aquilegia Petal Spur.” *Proceedings. Biological Sciences* 282 (1803): 20142778.
Yuan, Yateng, Xiaotong Ou, Minhao Yao, Pinle Wang, Chunlian Li, Guisen Zhang, Mengqi He, et al. 2025. “GT1 and ZmHB13/VRL1 Regulate Flower Sexual Differentiation by Modulating Jasmonate Biosynthesis and Signaling in Maize.” *Plant Physiology* 197 (3): kiaf075.
Yuxin Wu, Alexander Kirillov, Francisco Massa, Wan-Yen Lo, Ross Girshick. 2019. “Detectron2.” 2019. https://github.com/facebookresearch/detectron2.
Zebell, Sophia G., Carlos Martí-Gómez, Blaine Fitzgerald, Camila Pinto Da Cunha, Michael Lach, Brooke M. Seman, Anat Hendelman, et al. 2025. “Cryptic Variation Fuels Plant Phenotypic Change through Hierarchical Epistasis.” *bioRxivorg*. https://doi.org/10.1101/2025.02.23.639722.

Zhang, Jianzhi. 2023. “Patterns and Evolutionary Consequences of Pleiotropy.” *Annual Review of Ecology, Evolution, and Systematics* 54 (1): 1–19.